NASA TN D-313

TECHNICAL NOTE
D-313

EFFECT OF LEADING-EDGE THICKNESS ON THE FLOW OVER A FLAT PLATE AT A MACH NUMBER OF 5.7

By Marcus O. Creager

Ames Research Center
Moffett Field, Calif.

NATIONAL AERONAUTICS AND SPACE ADMINISTRATION

WASHINGTON

May 1960

NATIONAL AERONAUTICS AND SPACE ADMINISTRATION

TECHNICAL NOTE D-313

EFFECT OF LEADING-EDGE THICKNESS ON THE FLOW OVER A FLAT PLATE AT A MACH NUMBER OF 5.7

By Marcus O. Creager

SUMMARY

The flow field over a flat plate with various leading-edge thicknesses was surveyed at a free-stream Reynolds number of 20,000 per inch. Impact-probe and surface static pressures were measured for a range of leading-edge thicknesses from 0.001 to 0.25 inch. The measured surface pressures compared unsatisfactorily with those values calculated from a linear combination of blast-wave and weak viscous interaction parameters.

For thin leading edges the boundary layer grew linearly near the leading edge. The tests were not sufficiently extensive to define the boundary layer and the shock wave very near the leading edge. The boundary layer was in a high entropy layer only for the thickest plates.

INTRODUCTION

Previous experimental results obtained for blunted bodies in hypersonic flow have indicated that in the vicinity of the leading edge the boundary layer grows in a high entropy layer generated by a strong or detached bow shock wave (refs. 1, 2, 3). The growth of the boundary layer as it becomes thicker than the high entropy layer has not been adequately described.

The purpose of the research described herein was to study experimentally the effect of leading-edge thickness on the flow field over a flat plate. In particular, it was hoped to obtain from the experimental results some indication of the growth of the boundary layer and the total pressure at the boundary-layer edge.

Experimental surface-pressure and impact-pressure distributions were obtained for flat plates in the Ames 8-Inch Low Density Wind Tunnel at a Mach number of 5.7.

SYMBOLS

b_∞	$\gamma\left[\frac{0.865}{M_\infty^2}\frac{T_w}{T_\infty} + 0.166(\gamma - 1)\right]$
B_∞	$\left(\frac{2b_\infty}{\gamma} M_\infty^2 + 4.27\right)\sqrt{C_w}$ (See eq. (1).)
C_w	constant in linear viscosity relation
d	leading-edge thickness (See fig. 1.)
h	height defined in sketch of appendix A
M	Mach number
p	static pressure
R	height of point on shock wave (See sketch in appendix A.)
Re_∞	unit Reynolds number, $\frac{\rho_\infty u_\infty}{\mu_\infty}$
T	temperature
u	velocity
x,y	coordinate lengths (See sketch in appendix A.)
β	angle defined in sketch of appendix A
γ	ratio of specific heats
δ	boundary-layer thickness
δ^*	boundary-layer displacement thickness
ρ	density

Subscripts

sw	quantity based on condition just behind shock wave
w	quantity based on body wall or surface condition
t_∞	total quantity based on undisturbed free-stream conditions
t_δ	local total quantity at the boundary-layer edge

t_{sw} local total quantity just downstream of shock wave

t_3 total quantity behind normal shock wave

δ quantity based on condition at boundary-layer edge

∞ quantity based on undisturbed free-stream conditions

TEST EQUIPMENT AND TEST METHOD

Equipment

The tests were conducted in the 8-Inch Low Density Wind Tunnel (ref. 3). The test conditions were a Mach number of 5.7 and free-stream Reynolds number of 20,000 per inch. The usable stream consisted of a core of about 2 inches in diameter (ref. 3).

Test body.- The thinnest leading edges were constructed of a 1/2-inch wide strip of either 0.001- or 0.002-inch gage stock attached to the upper surface of a 1/4-inch-thick plate (see fig. 1). Gage stock cemented to the 0.002-inch piece gave additional thickness (see inset fig. 1). (The cylindrical leading-edge plate used as the base body here was the test body described in ref. 3.) The leading edges were square with thickness from 0.001 to 0.0625 inch. Two cylindrical leading edges were also tested with leading-edge thicknesses of 0.0625 and 0.25 inch. The plate surface pressure orifices were connected to a multiple tube manometer. A cathetometer was used to locate and measure the manometer oil level heights.

Probe.- The impact pressure probe (ref. 3) was constructed of stainless-steel tubing flattened to an oval shape of 0.016-inch height. The impact pressures sensed by this probe were indicated by an oil manometer. The free-stream Reynolds number based on probe height was about 320. According to references 4 and 5, the viscous correction applicable to the reading obtained by the probe is negligible for locations greater than two to three probe heights above the plate surface.

Test Method

The surface pressures were obtained at one stream condition for the range of leading-edge thickness from 0.001 to 0.0625 inch.

The impact pressures were obtained by traversing the probe in a direction normal to the plate surface. The surveys were performed above the pressure orifices of the plates. The traverses were extended to the shock wave, although probe pressures were not obtained in detail in the vicinity of the shock wave. The probe axis was alined with the free-stream direction.

RESULTS AND DISCUSSION

Impact-Pressure Surveys

A typical impact-pressure profile is presented in figure 2. Near the plate surface, the impact pressure increases rapidly with distance above the plate. This region is identified as the boundary layer. The increase of impact pressure with distance is less above the boundary layer than in the boundary layer, and impact pressure reaches a peak value at the shock wave. The method described by Kendall (ref. 6) is used to define the boundary-layer edge as the intersection of the two straight lines shown in figure 2.

In figures 3(a) through 3(j), the measured impact pressures, p_{t_3}, are plotted versus height, y, of the probe above the plate surface. The profiles corresponding to locations near the leading edge (small values of x) exhibit such a large gradient of impact pressure outside the boundary-layer region that it is difficult to determine the edge of the boundary layer. Farther aft (large values of x) the profiles exhibit a smaller gradient between the boundary-layer region and the shock wave. The profiles in figures 3(h) and 3(j) were obtained for plates with cylindrical leading edges; the other profiles of figure 3 were obtained for square leading edges.

Boundary-Layer Thickness

The boundary-layer heights versus distance from the leading edge are presented in figure 4 for d = 0.001 to 0.25 inch. Forward of 3 inches, the data compare favorably with the solid line calculated by the following equation for boundary-layer growth over a sharp plate in hypersonic viscous flow (ref. 3):

$$\delta = \frac{B_\infty x}{\sqrt{Re_\infty x}} \qquad (1)$$

where

$$B_\infty \equiv \left(\frac{2b_\infty M_\infty^2}{\gamma} + 4.27\right)\sqrt{C_w}$$

It should be noted, however, that the data exhibit a weak dependence on leading-edge thickness; the boundary-layer height increases as the leading-edge thickness is increased from 0.001 to 0.014 inch.

The boundary-layer heights are presented in figure 5, in ratio to plate leading-edge thickness. The details of the boundary-layer growth rate are brought out more fully by this type of plot. For instance, the data for $d = 0.001$ inch indicate a linear growth of the boundary layer with distance x near the leading edge, and the parabolic growth occurs only farther aft. This type of variation is characteristic of the data for $d = 0.001$ to 0.014 inch.

Shock-Wave Shape

The shock-wave coordinates were obtained during the flow field surveys with the impact-pressure probe. In figure 6 the shock-wave heights measured above the plate surface are plotted versus the distance x from the leading edge. The present data for values of d from 0.001 to 0.010 inch lie very close together. In figure 6 for larger values of d, the shock wave may be noted to steepen and to occur at larger distances above the plate surface.

The shock-wave coordinates are presented in figure 7 as multiples of the leading-edge thickness d. Here the height R is measured from the center-line plane of the leading edge. Also plotted in figure 7 is a solid line calculated from the following equation:

$$\left(\frac{R}{d}\right)^2 = 5.3\,\frac{x}{d} + 0.07\left(\frac{x}{d}\right)^2 \qquad (2)$$

The form of equation (2) was arbitrarily selected and the constants were empirically determined. The shock-wave equation from equation (17) of reference 3 for zero sweep and negligible standoff distance is:

$$\frac{R}{d} = 1.3\left(\frac{x}{d}\right)^{2/3} \qquad (3)$$

The dashed line in figure 7 was calculated from equation (3) and is noted to be in fair agreement with the data only for values of x/d less than 100.

Surface Pressures

The measured surface pressures in ratio to the free-stream static pressure are plotted versus x in figure 8 for a range of leading-edge thicknesses. The pressures decrease with distance from the leading edge and, in general, the variation of surface pressures with leading-edge thickness for a given value of x is not systematic. For most values of x the pressures measured on the plate with a cylindrical and a square leading edge of 0.0625-inch thickness are in agreement. These pressures were obtained in the regime of weak interaction where $M_\infty^3/\sqrt{Re_{\infty x}}$ is small and the prediction scheme (ref. 2) of using a viscous term in linear combination with an inviscid term is only of qualitative value. The following equation can be obtained from equation (6) of reference 2:

$$\frac{p}{p_\infty} = 1 + 0.32\frac{M_\infty^3}{\sqrt{Re_{\infty x}}} + 0.1\frac{M_\infty^2}{(x/d)^{2/3}} \qquad (4)$$

The terms of equation (4) were calculated from free-stream conditions for the plate where $d = 0.001$ and 0.0625 inch. The results are plotted as indicated in figure 8. Note that this crude method has some merit in that the data compare fairly well to the corresponding calculated values. A more exact comparison necessarily awaits better definition of the flow field over these bodies.

Boundary-Layer-Edge Total Pressure

The variation of entropy along the boundary-layer edge depends on both the boundary-layer growth and shock-wave shape. Boundary-layer growth is primarily an x distance phenomenon and the shape of the shock wave is dependent on both x distance and leading-edge thickness d. The variation of total pressure calculated across the shock wave described by equation (2) (for the present test conditions) is presented in figure 9.

The measured impact pressure was obtained at the arbitrarily defined boundary-layer edge. If one assumes constant static pressure through the boundary layer, a value of the local total pressure at the boundary-layer edge may be calculated.

Such a calculation was performed for the present data. The results are presented in figure 10 where the total pressure, in ratio to the free-stream value, is plotted versus the dimensionless distance from the leading edge, x/d. The general observation can be made from figure 10 that the boundary layer is in a high entropy layer for the thickest plates and is not in the high entropy layer for the thin plates. (The apparent abrupt rise in $p_{t_\delta}/p_{t_\infty}$ with increase in x/d may not be realistic.)

The method outlined in appendix A for the theoretical parabolic boundary-layer growth was used to estimate the variation of local total pressure, p_{t_δ}, with x/d for $Re_{\infty d}$ = 4860, 1250, 280, and 20. The results are presented as solid lines in figure 10. The data for $Re_{\infty d}$ = 4860, 1250, and 20 compare favorably with the solid lines for values of x/d less than 50, but the line for $Re_{\infty d}$ = 280 does not fit the experimental results. The curve of figure 9 (i.e., $p_{t_{sw}}/p_{t_\infty}$ vs. R/d) is very similar to the arrangement of the data points in figure 10 (i.e., $p_{t_\delta}/p_{t_\infty}$ vs. x/d). A casual observation at this point would be that, if the effect of $Re_{\infty d}$ is ignored, a comparison between theory and experiment for figure 10 might be accomplished if equation (A9) is replaced by a linear variation such as $h/d \sim x/d$. This implies a linear growth of the boundary layer similar to that noted for the thin plates (d = 0.001 to 0.014 in the discussion of figure 5. The dashed line was calculated for such a linear variation where $h/d = 0.061(x/d)$. However, the results for boundary-layer growth over the thick plate ($Re_{\infty d}$ = 4860) do not seem to substantiate the possibility that one single curve of $p_{t_\delta}/p_{t_\infty}$ vs. x/d should correlate the results over the range of conditions of figure 10. Thus, the dashed curve presented in figure 10 does not provide a universal correlation. The exact calculation of curves of this type is dependent on a more realistic representation of the flow than is possible with the present data. Surveys closer to the leading edge of thin plates and farther aft on blunt plates would be valuable for this type of comparison. In addition, boundary-layer data obtained on a plate of fixed leading-edge thickness for a wide range of low unit Reynolds numbers would contribute greatly to the development of an over-all correlation.

CONCLUDING REMARKS

An impact pressure probe was used to examine the flow field over a plate at M_∞ = 5.7 and Re_∞ = 20,000 per inch. The boundary layer grew out of the high entropy layer as the leading-edge thickness was varied from 0.25 to 0.001 inch. For blunt plates, where $Re_{\infty d}$ was greater than 1250, the boundary layer developed in the high entropy layer over the test length. For $Re_{\infty d}$ less than 150, the boundary-layer edge aft of x = 0.5 inch was in a low entropy layer. For the $Re_{\infty d}$ values between 150 and 1250, data obtained near the leading edge indicated possible emergence of the boundary layer out of the high entropy layer. For the thinnest leading edges the boundary-layer growth was linear with distance from the leading edge. The evidence is neither sufficiently accurate nor sufficiently extensive to permit quantitative evaluation.

Surface pressures were found to vary with distance along the surface and with leading-edge thickness. They were not satisfactorily predicted by a linear combination of viscous and inviscid effects.

The data obtained herein on boundary-layer growth rate and shock-wave development were insufficient to establish a truly consistent flow model for correlation of these data.

Ames Research Center
National Aeronautics and Space Administration
Moffett Field, Calif., Jan. 7, 1960

APPENDIX A

CALCULATION OF LOCAL TOTAL PRESSURE

The possible theoretical flow model used for this calculation scheme is pictured in the following sketch.

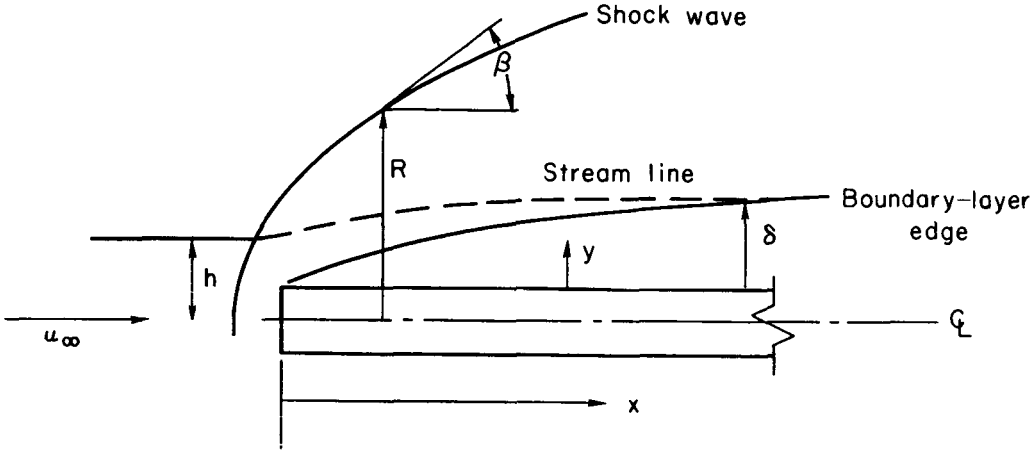

The mass flow of the free stream may be calculated by

$$m_\infty = \rho_\infty u_\infty h \tag{A1}$$

The mass flow in the boundary layer at a distance x from the leading edge may be found simply by

$$m_\delta = \int_0^\delta \rho u \, dy \tag{A2}$$

It is assumed that the mass of fluid contained in the height h is found at x in the boundary-layer thickness δ and that a streamline originating at h enters the boundary-layer edge at x. Then

$$\rho_\infty u_\infty h = \int_0^\delta \rho u \, dy$$

and

$$h = \int_0^\delta \frac{\rho u}{\rho_\infty u_\infty} \, dy \tag{A3}$$

Also by definition of the boundary-layer displacement thickness

$$\delta^* = \delta - \int_0^\delta \frac{\rho u}{\rho_\delta u_\delta}\, dy \tag{A4}$$

Then combining (A3) and (A4) yields

$$h = (\delta - \delta^*)\frac{\rho_\delta u_\delta}{\rho_\infty u_\infty} \tag{A5}$$

Equation (A5) may be rewritten as

$$\frac{h}{d} = \left(\frac{\delta}{d} - \frac{\delta^*}{d}\right)\frac{\rho_\delta u_\delta}{\rho_\infty u_\infty} \tag{A6}$$

The boundary-layer thickness formula of reference 3 (based on free-stream condition for a first approximation) is

$$\frac{\delta}{d} = \frac{B_\infty}{\sqrt{Re_{\infty d}}}\sqrt{\frac{x}{d}} \tag{A7}$$

The corresponding formula for the displacement thickness is

$$\frac{\delta^*}{d} = \frac{2b_\infty M_\infty^2}{\gamma\sqrt{Re_{\infty d}}}\sqrt{\frac{C_w x}{d}} \tag{A8}$$

Then substitution of equations (A7) and (A8) into equation (A6) yields

$$\frac{h}{d} = \frac{4.27\sqrt{C_w}}{\sqrt{Re_{\infty d}}}\left(\frac{\rho_\delta u_\delta}{\rho_\infty u_\infty}\right)\sqrt{\frac{x}{d}} \tag{A9}$$

Without prior knowledge of $(\rho_\delta u_\delta)$ this quantity will be assumed equal to $(\rho_\infty u_\infty)$. If the shock-wave shape can be expressed as

$$\left(\frac{R}{d}\right)^2 = K_1\left(\frac{x}{d}\right) + K_2\left(\frac{x}{d}\right)^2 \tag{A10}$$

then the shock-wave angle is

$$\tan\beta = \frac{\sqrt{K_1^2 + 4K_2(h/d)^2}}{h/d} \tag{A11}$$

The total-pressure ratio across the shock wave is calculated from the equation below (for air)

$$\frac{p_{t_{sw}}}{p_{t_\infty}} = \left(\frac{6M_\infty^2\sin^2\beta}{M_\infty^2\sin^2\beta+5}\right)^{7/2}\left(\frac{6}{7M_\infty^2\sin^2\beta-1}\right)^{5/2} \tag{A12}$$

The use of equations (A9), (A11), and (A12) permits calculation of $p_{t_\delta}/p_{t_\infty}$ as a function of x/d and $Re_{\infty d}$.

REFERENCES

1. Kubota, Toshi: Investigation of Flow Around Simple Bodies in Hypersonic Flow. GALCIT Memo No. 40, June 25, 1957.

2. Creager, Marcus O.: Effects of Leading Edge Blunting on the Local Heat Transfer and Pressure Distribution Over Flat Plates in Hypersonic Flow. NACA TN 4142, 1957.

3. Creager, Marcus O.: The Effect of Leading Edge Sweep and Surface Inclination on the Hypersonic Flow Field Over a Blunt Flat Plate. NASA MEMO 12-26-58A, 1959.

4. Sherman, F. S.: New Experiments on Impact Pressure Interpretations in Supersonic and Subsonic Rarefied Airstreams. Univ. of Calif., Inst. of Eng. Res., Rep. HE - 150 - 99, Dec. 21, 1951.

5. Matthews, Malcolm L.: An Experimental Investigation of Viscous Effects on Static and Impact Pressure Probes in Hypersonic Flow. GALCIT Memo No. 44, June 2, 1958.

6. Kendall, James M., Jr.: Experimental Investigation of Leading-Edge Shock Wave Boundary Layer Interaction at Hypersonic Speeds. IAS Preprint No. 611, 1956 (Also Published as GALCIT Memo No. 30).

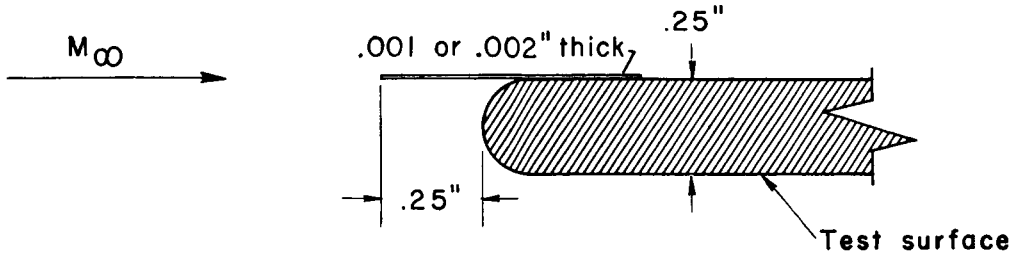

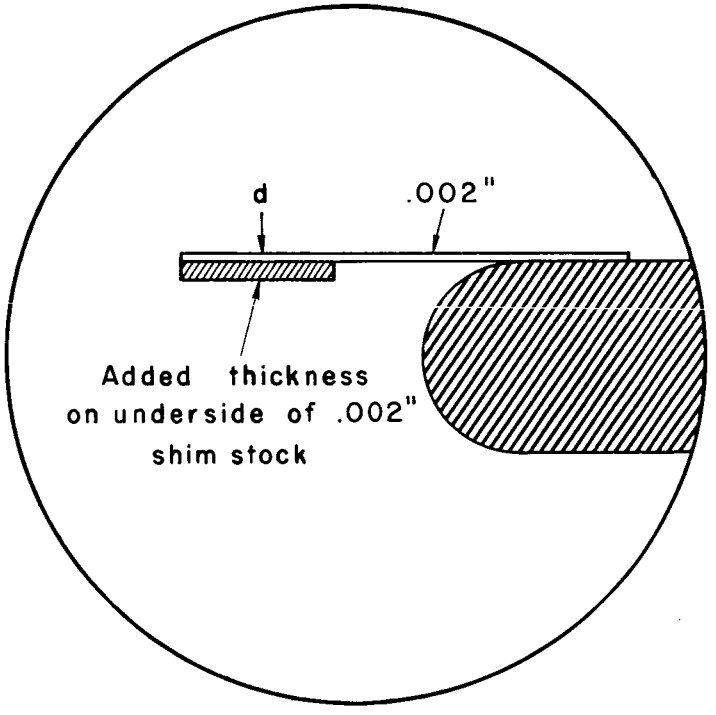

Figure 1.- Test body.

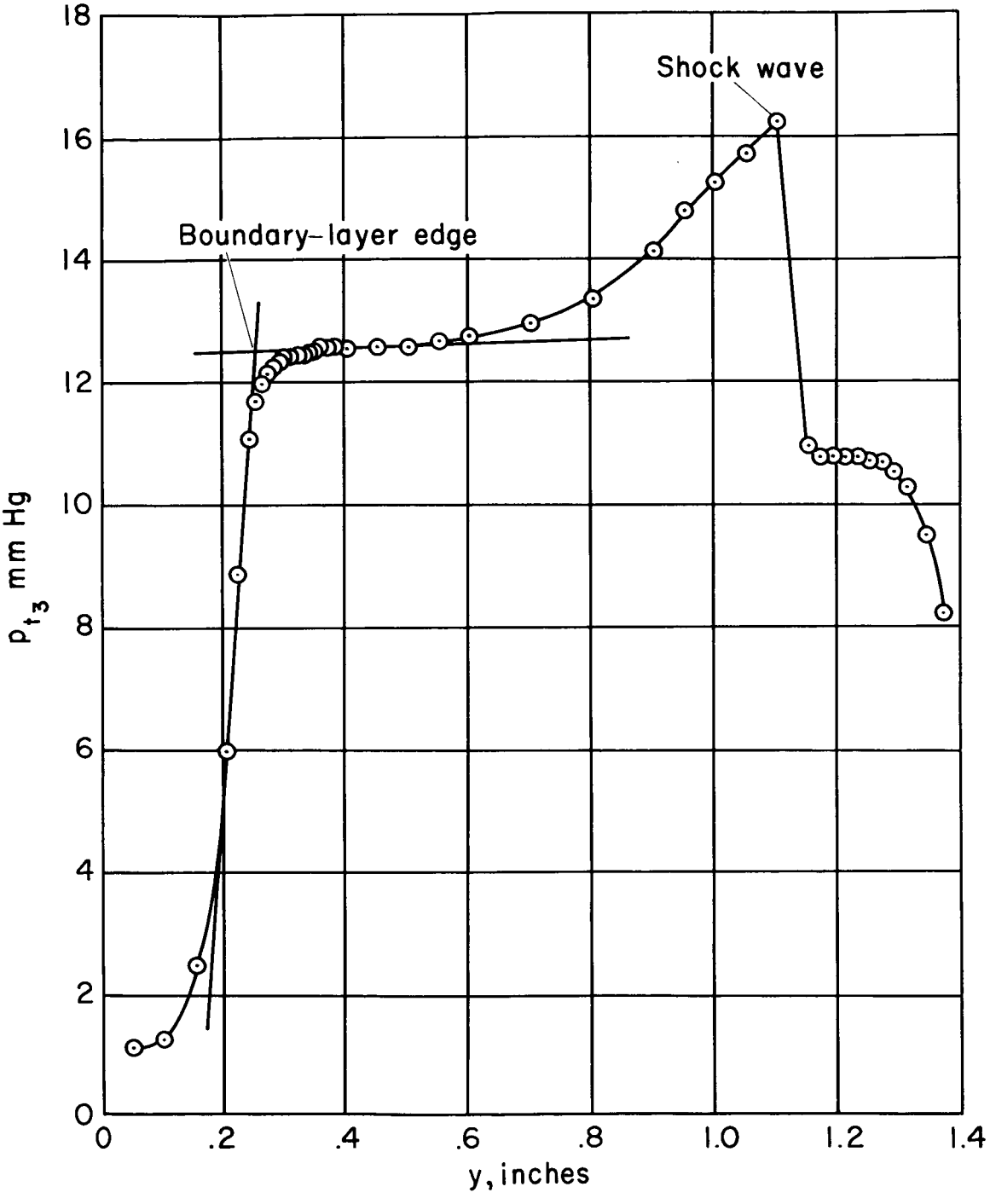

Figure 2.- Typical impact pressure profile; $M_\infty = 5.7$, $Re_\infty = 20{,}000$ per inch, d = 0.002 inch, x = 4.3 inch.

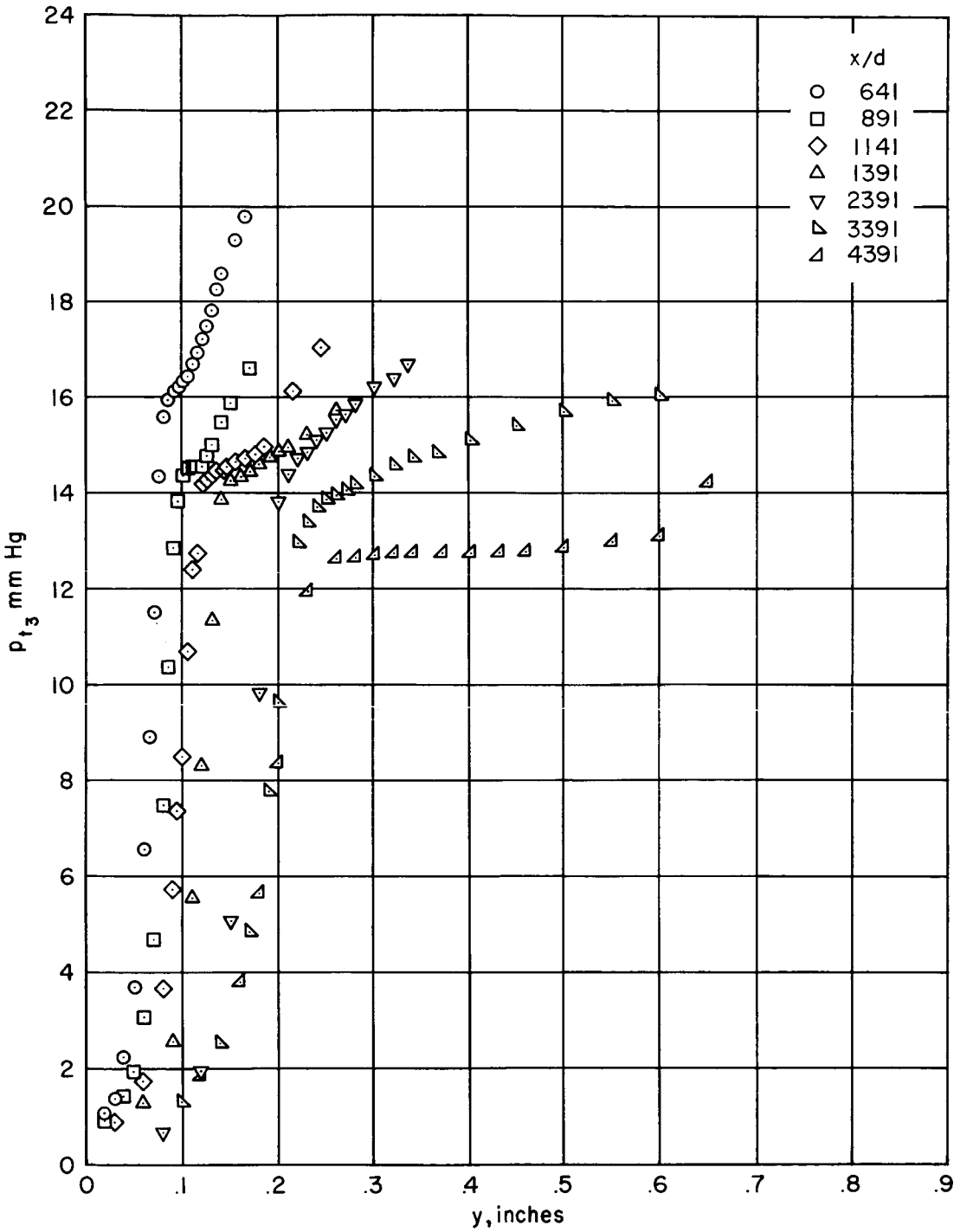

(a) d = 0.001 inch.

Figure 3.- Variation of measured impact pressure with distance above plate surface; $M_\infty = 5.7$, $Re_\infty = 20{,}000$ per inch.

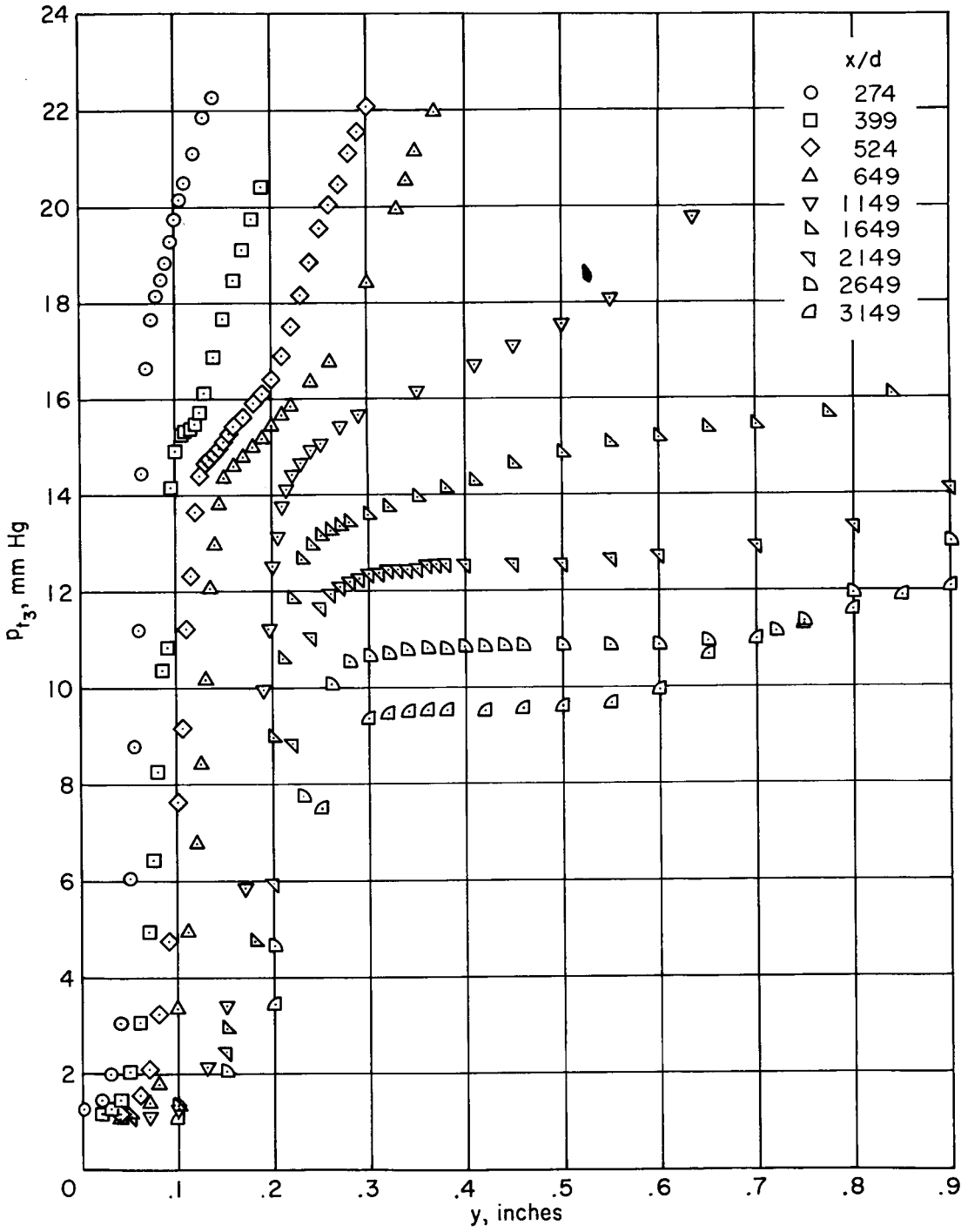

(b) d = 0.002 inch.

Figure 3.- Continued.

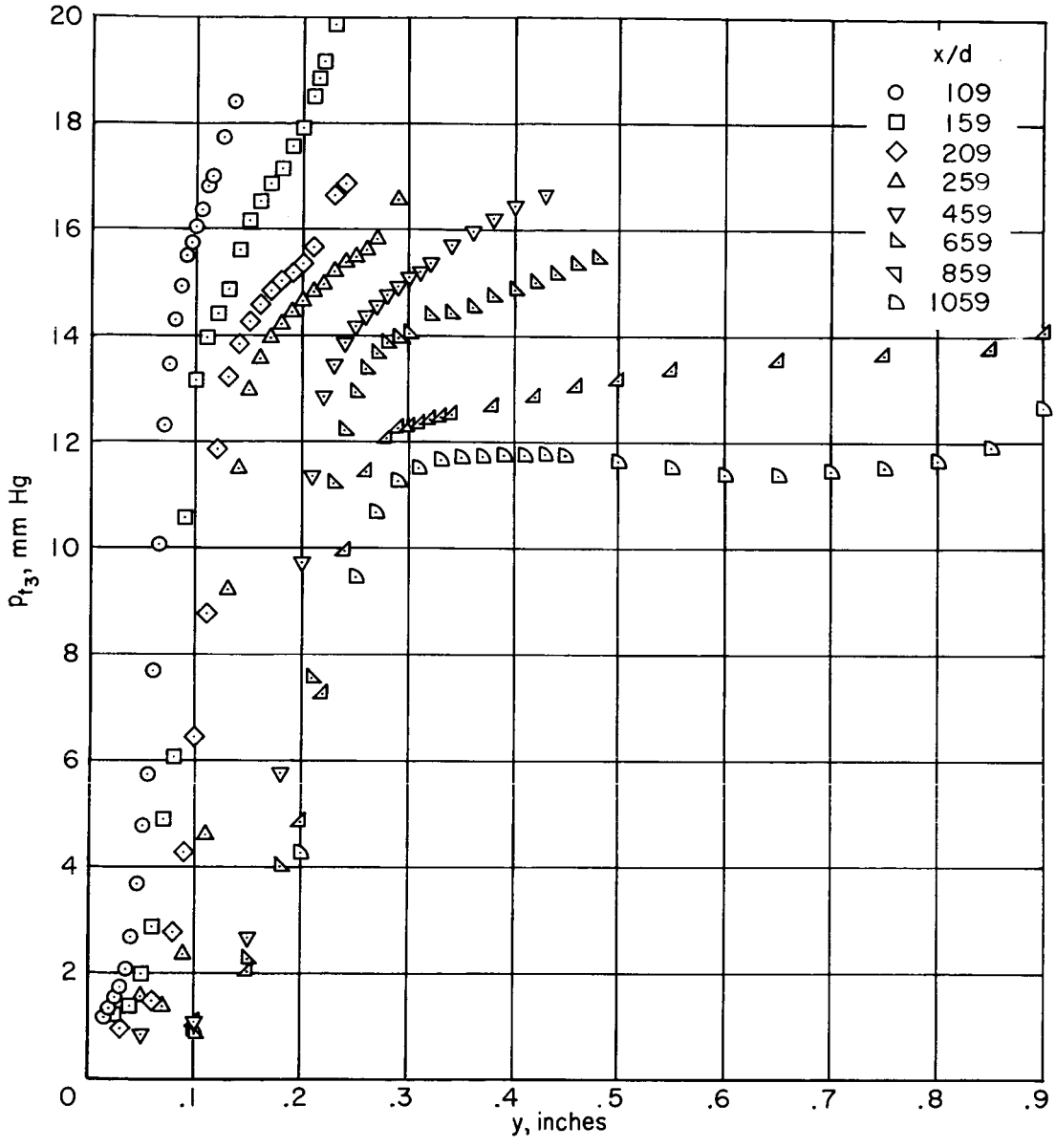

(c) d = 0.005 inch.

Figure 3.- Continued.

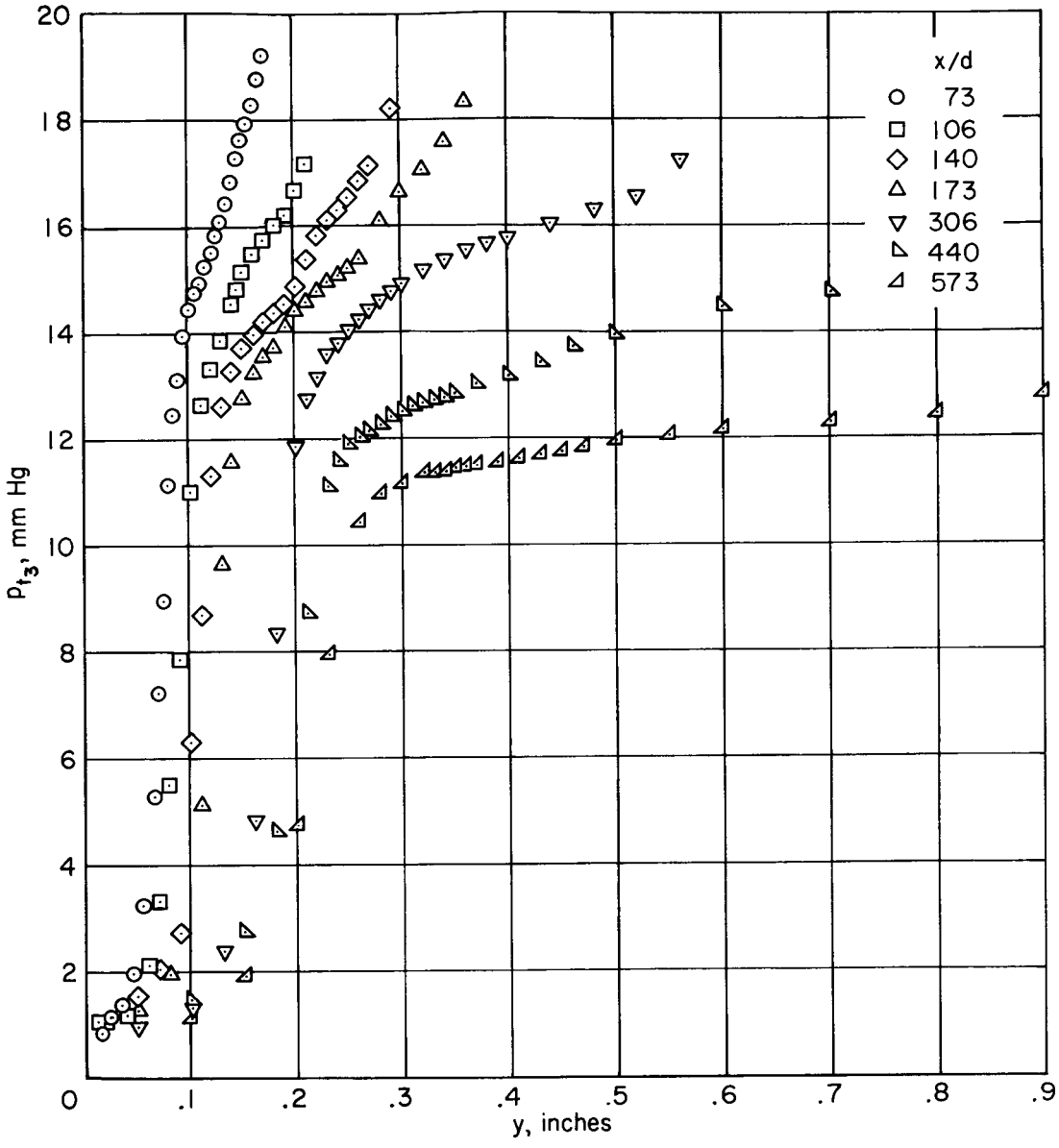

(d) d = 0.0075 inch.

Figure 3.- Continued.

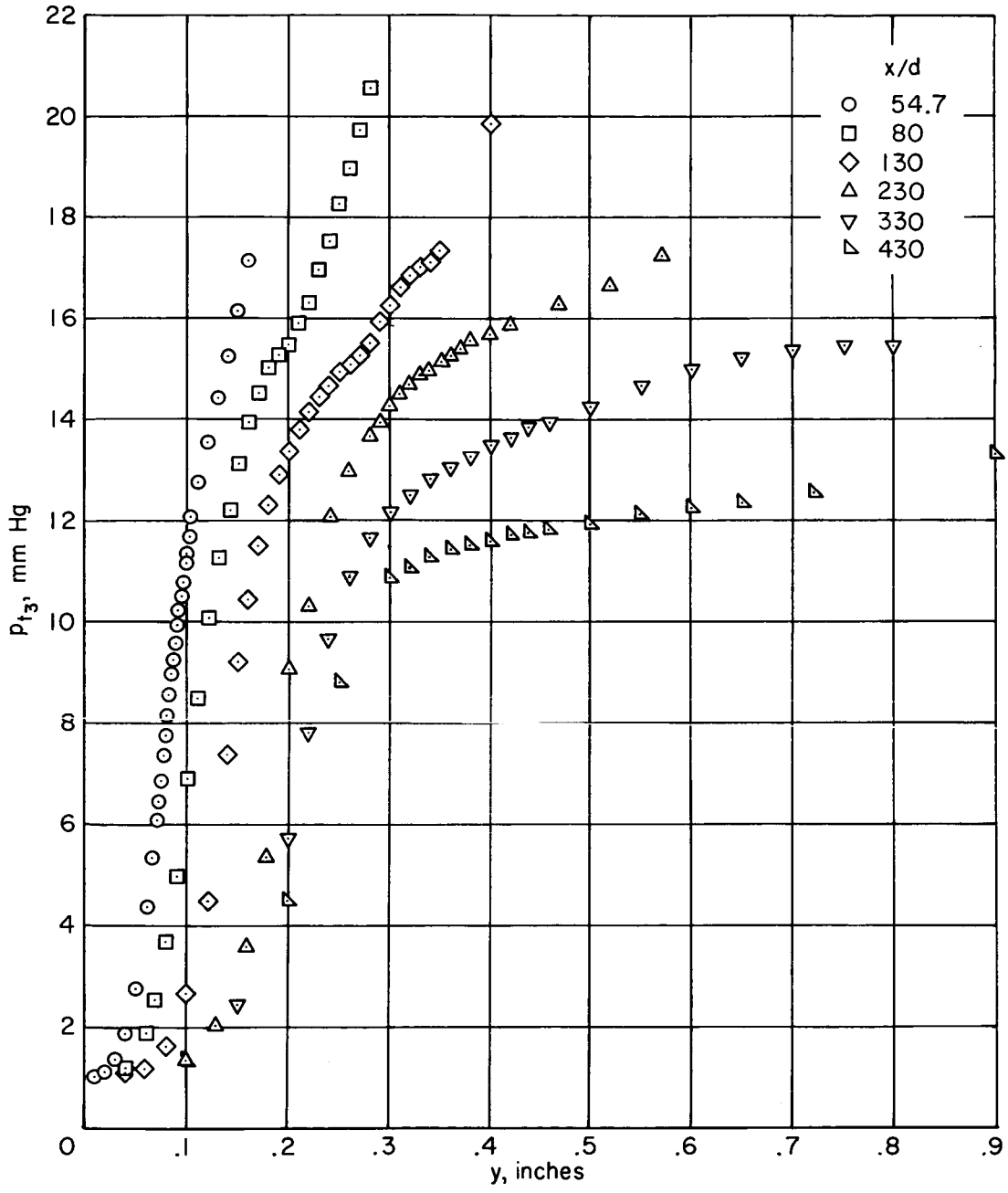

(e) d = 0.010 inch.

Figure 3.- Continued.

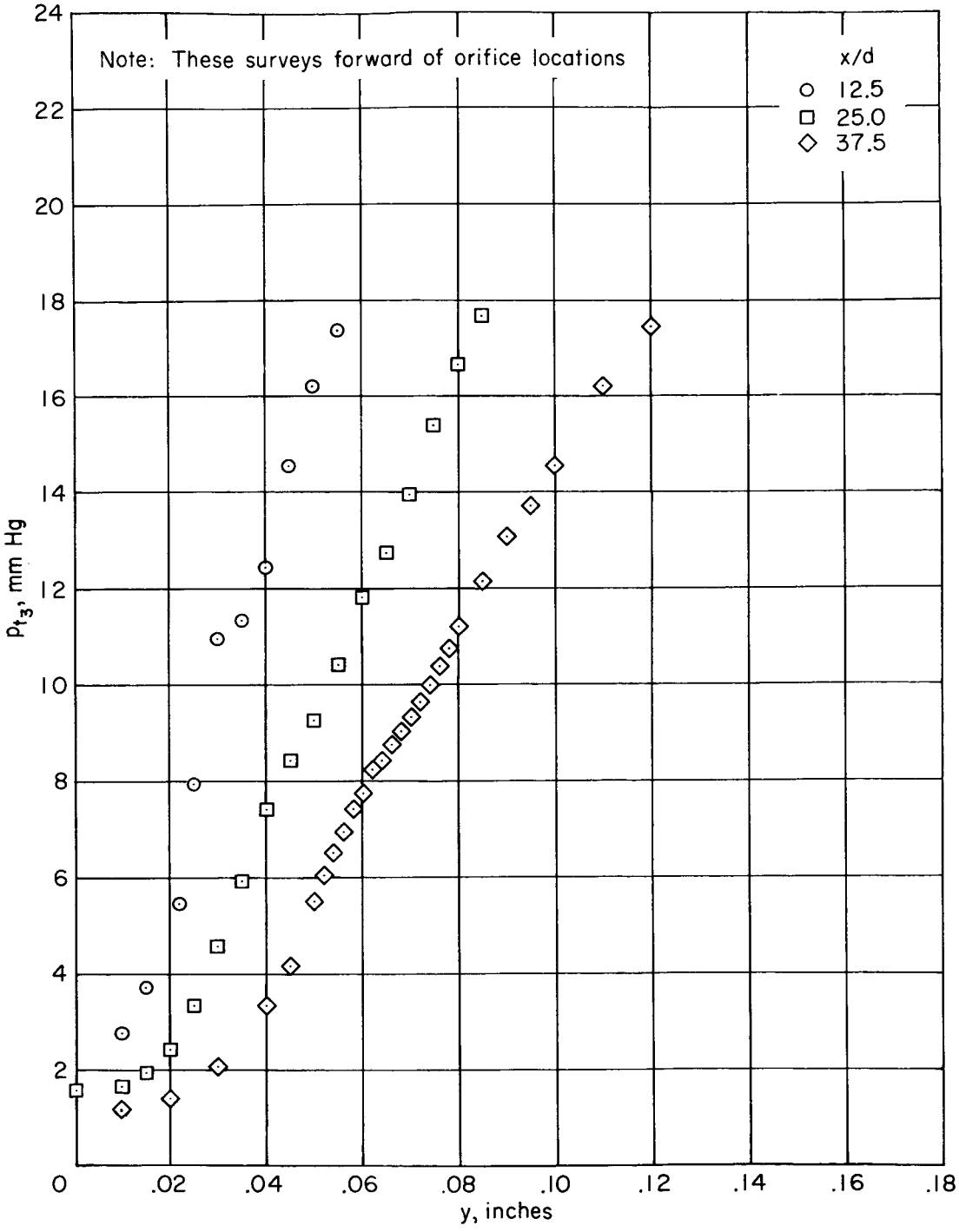

(f) d = 0.010 inch.

Figure 3.- Continued.

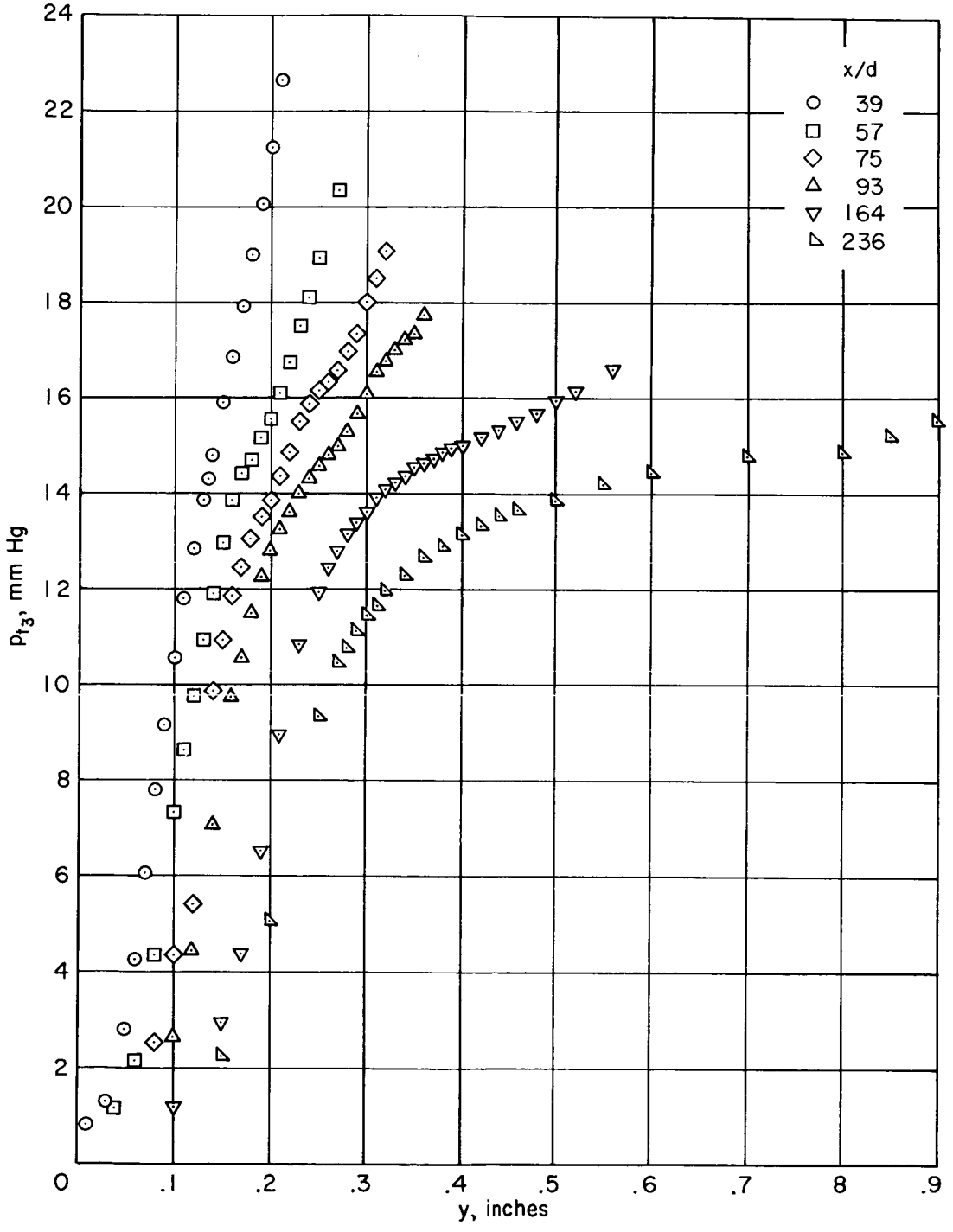

(g) d = 0.014 inch.

Figure 3.- Continued.

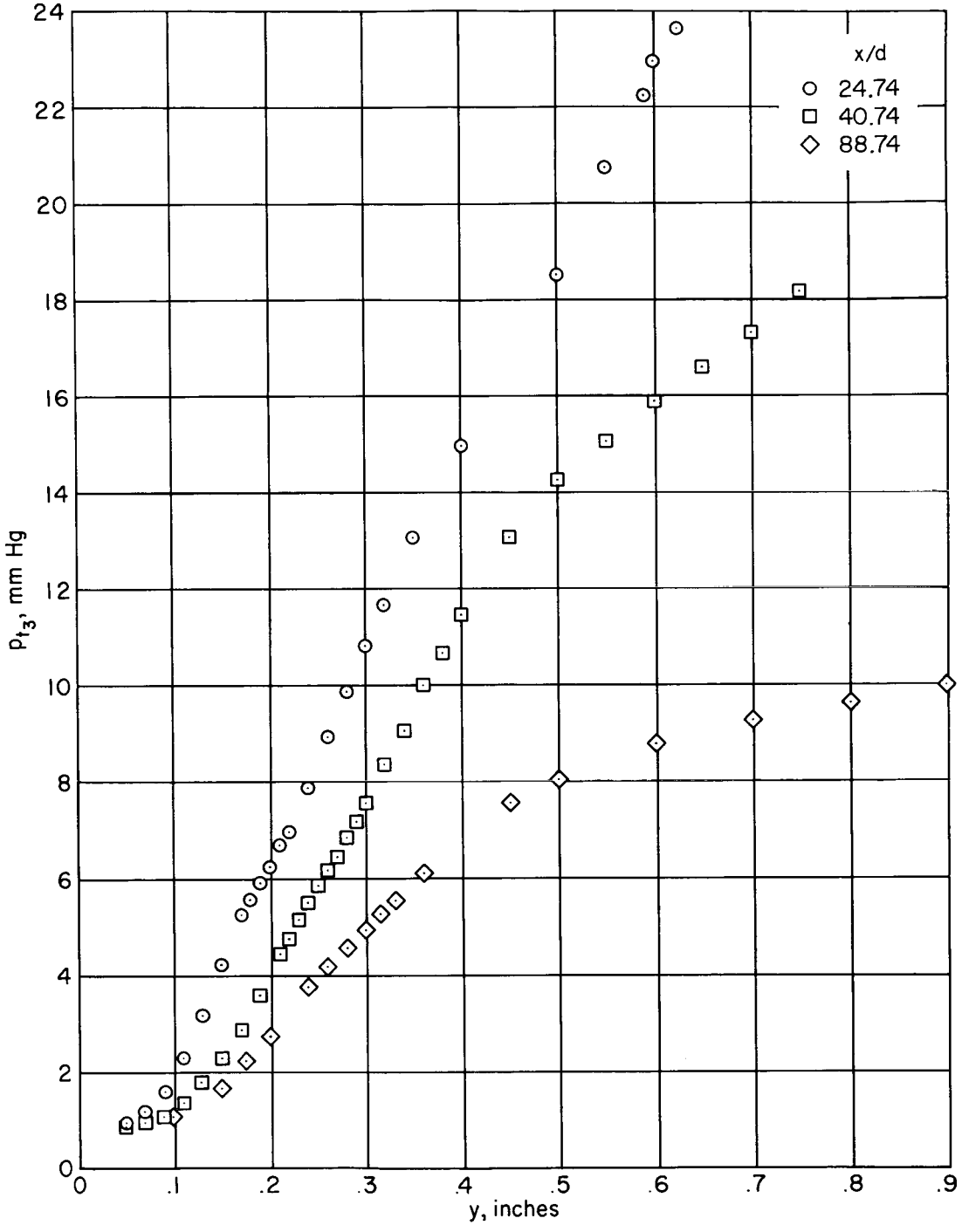

(h) d = 0.0625 inch (cylinder).

Figure 3.- Continued.

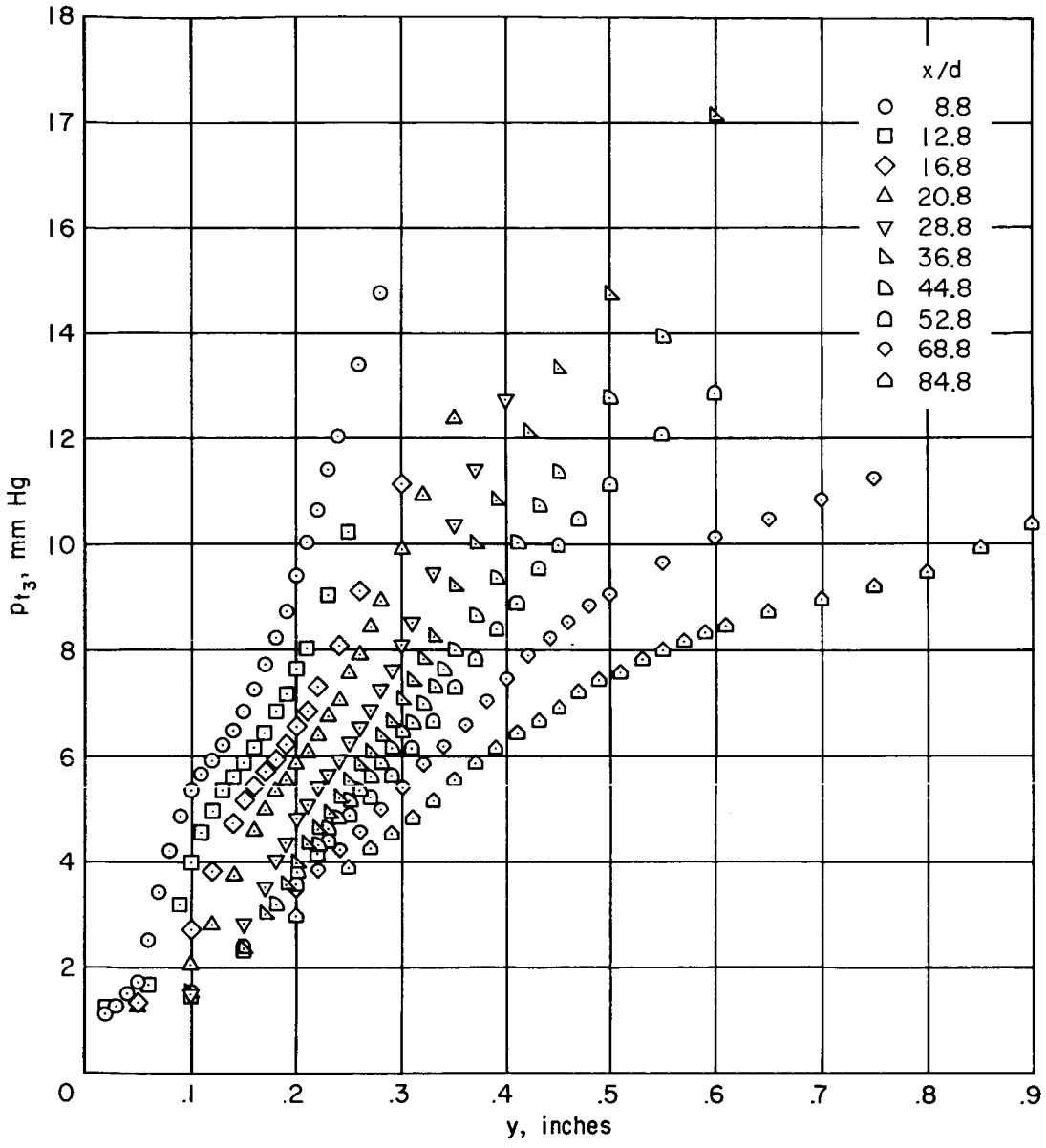

(i) d = 0.0625 inch.

Figure 3.- Continued.

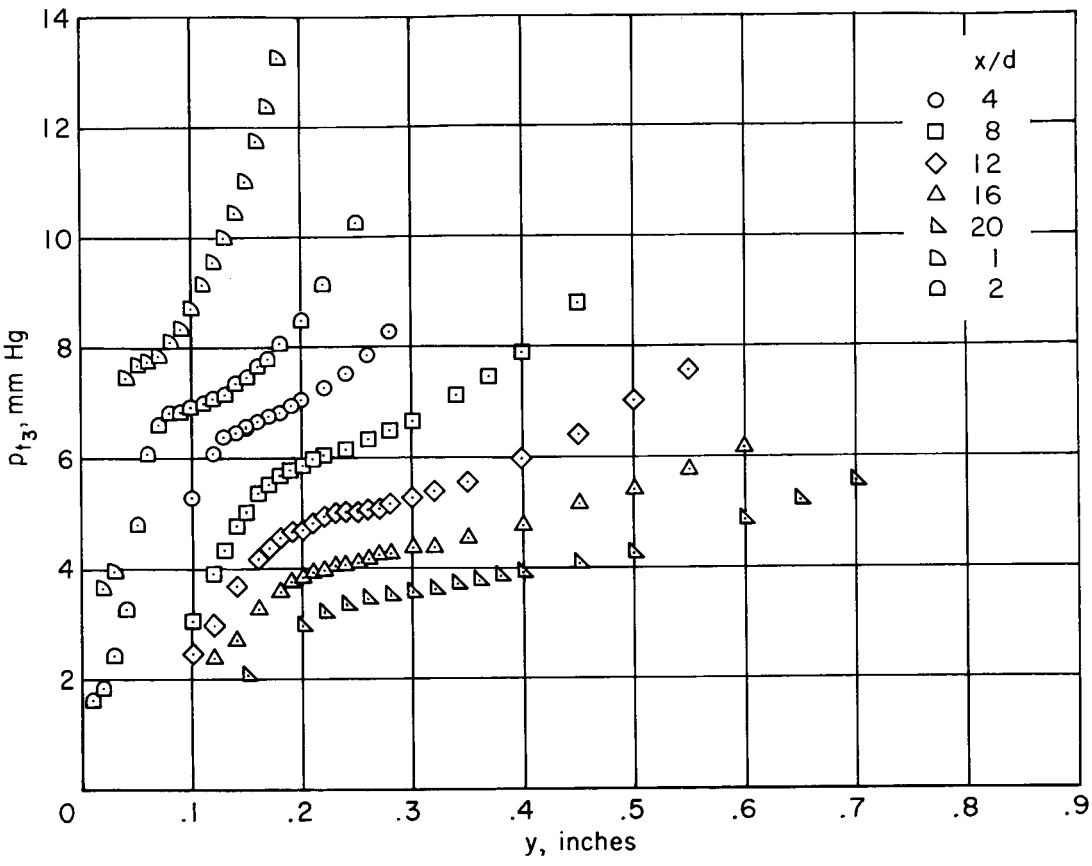

(j) d = 0.25 inch (cylinder).

Figure 3.- Concluded.

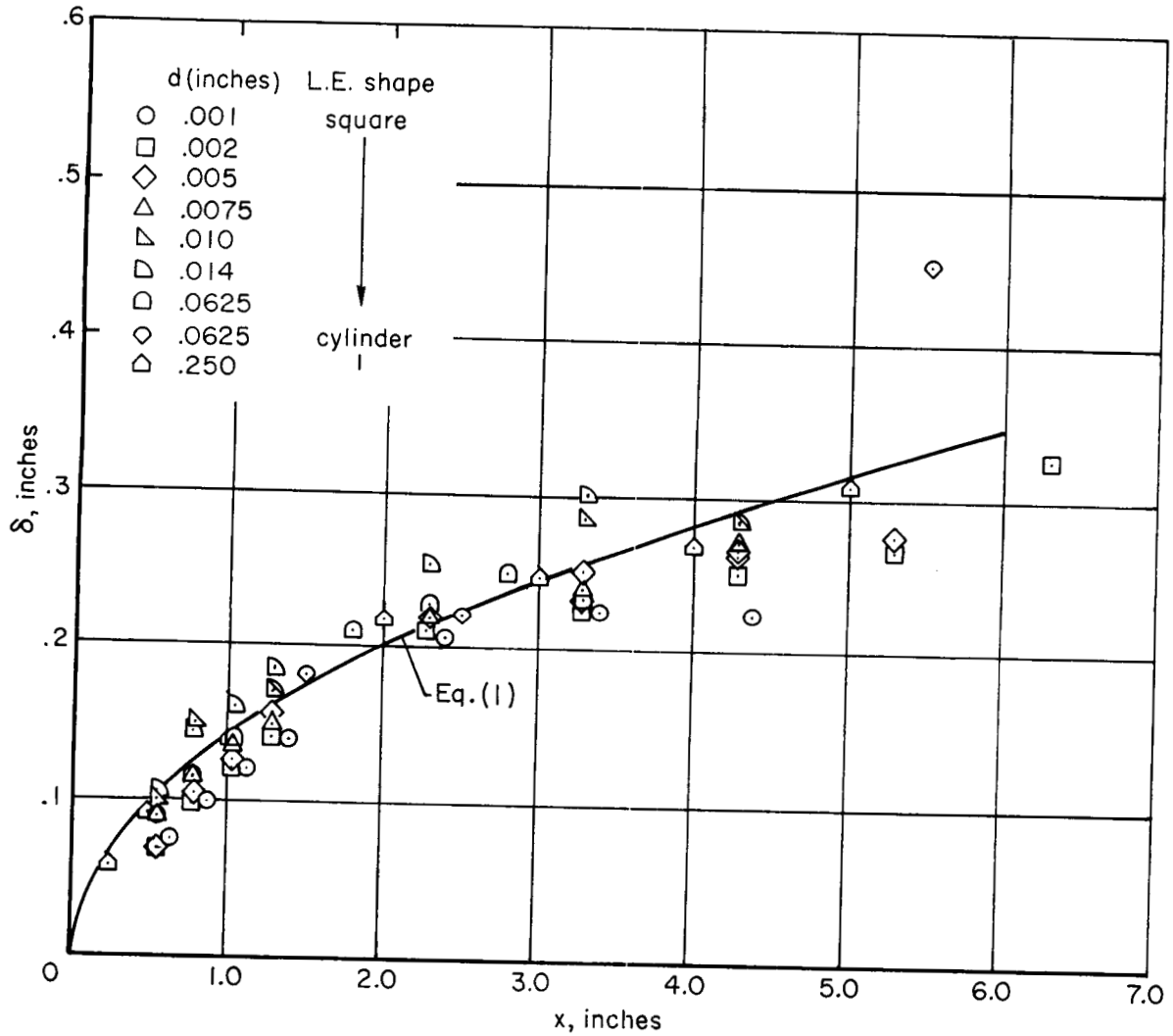

Figure 4.- Variation of boundary-layer height with distance from leading edge of flat plate; $M_\infty = 5.7$, $Re_\infty = 20{,}000$ per inch.

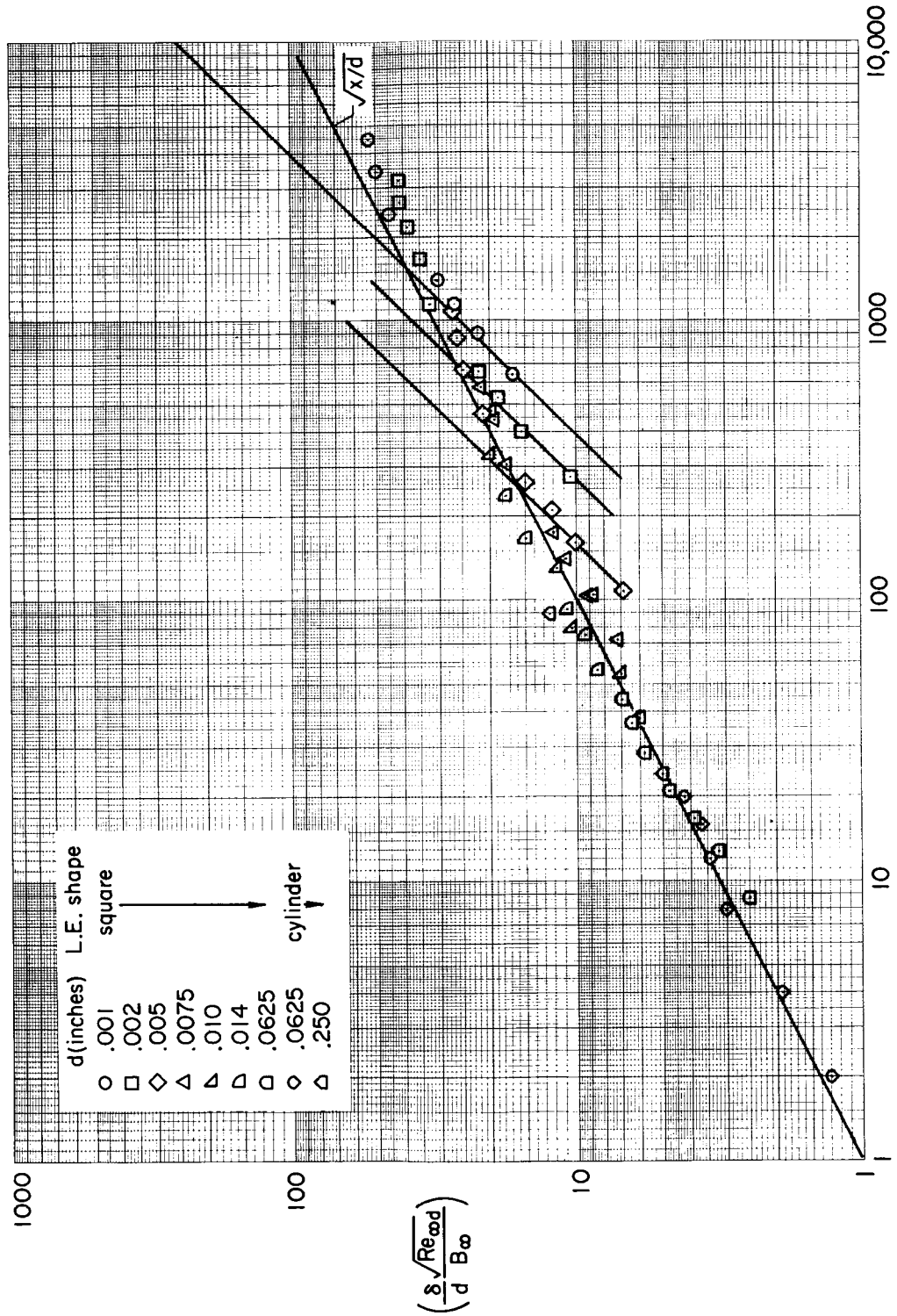

Figure 5.- Correlation of normalized boundary-layer height with normalized distance from the leading edge; $M_\infty = 5.7$, $Re_\infty = 20{,}000$ per inch.

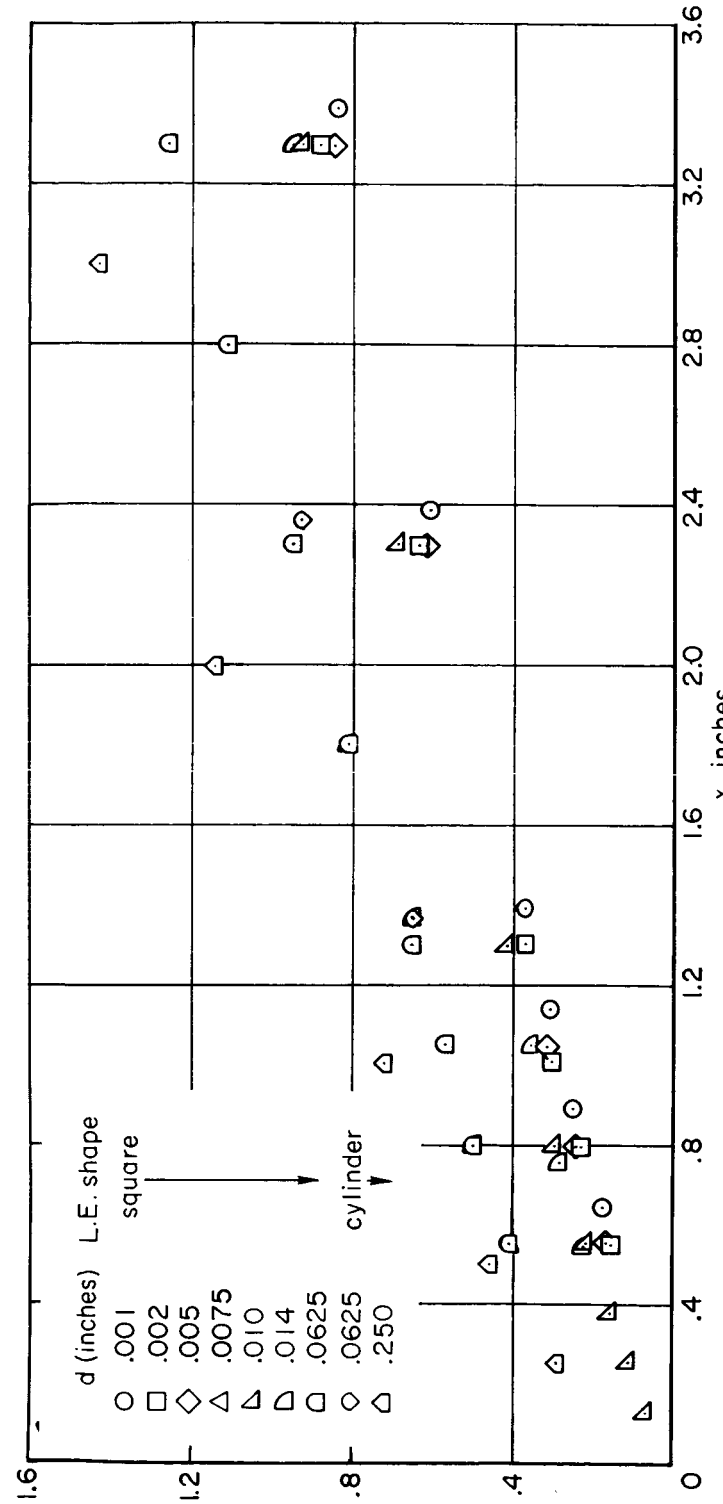

Figure 6.- Shock-wave coordinates for plates of different leading-edge thickness; $M_\infty = 5.7$, $Re_\infty = 20{,}000$ per inch.

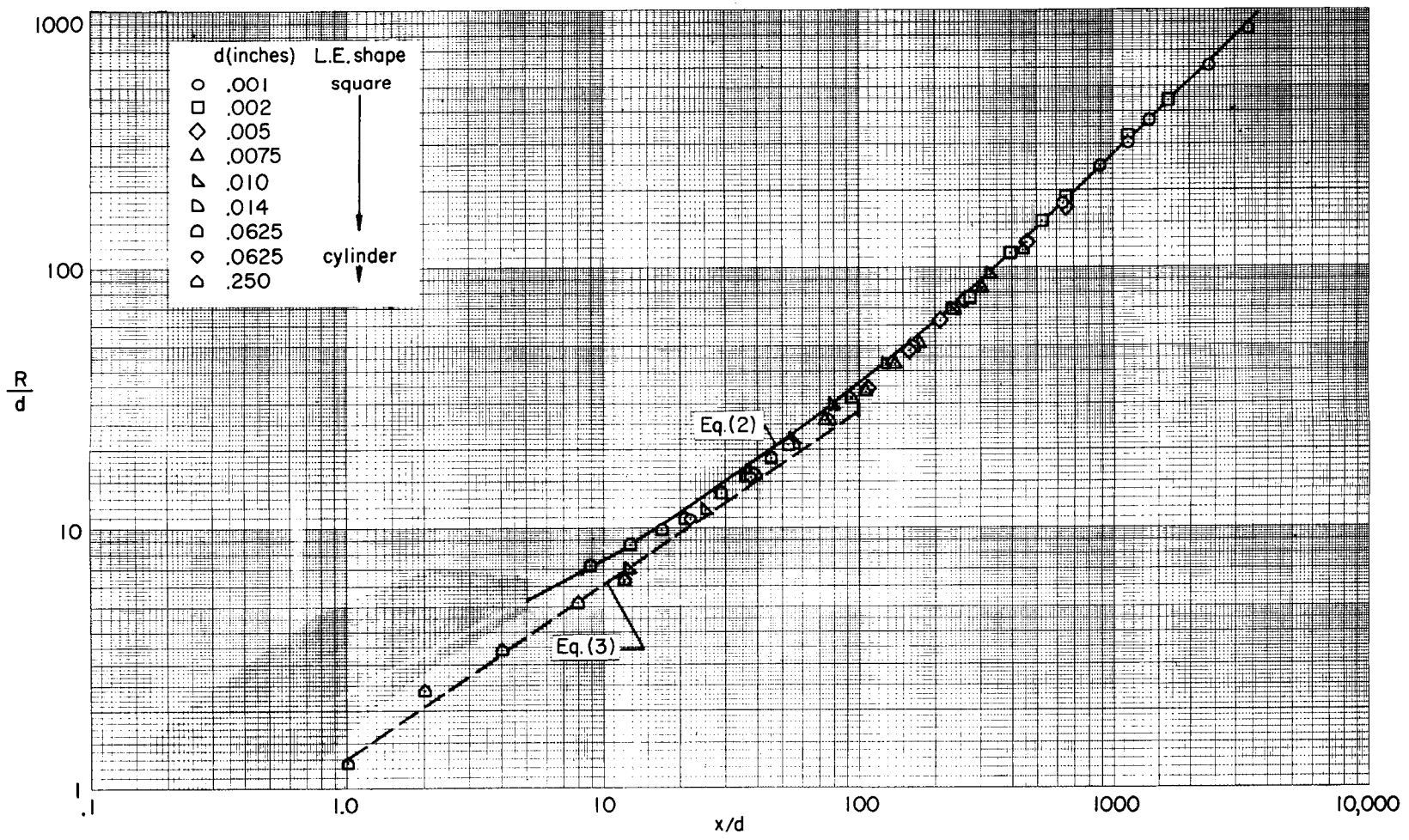

Figure 7.- Correlation of shock-wave coordinates; $M_\infty = 5.7$, $Re_\infty = 20{,}000$ per inch.

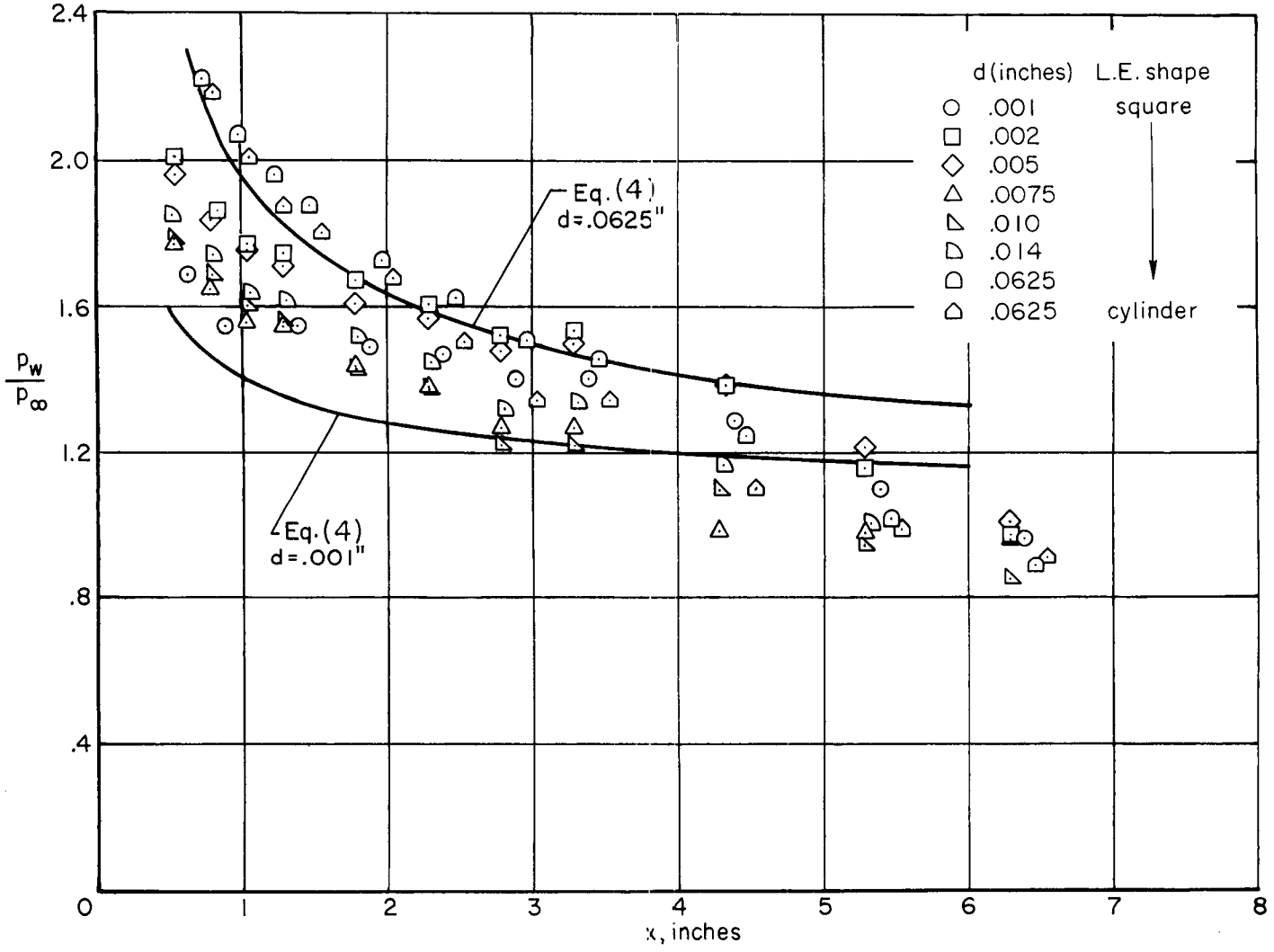

Figure 8.- Variation of the ratio of surface pressure to free-stream pressure with distance from the leading edge of a flat plate; $M_\infty = 5.7$, $Re_\infty = 20{,}000$ per inch.

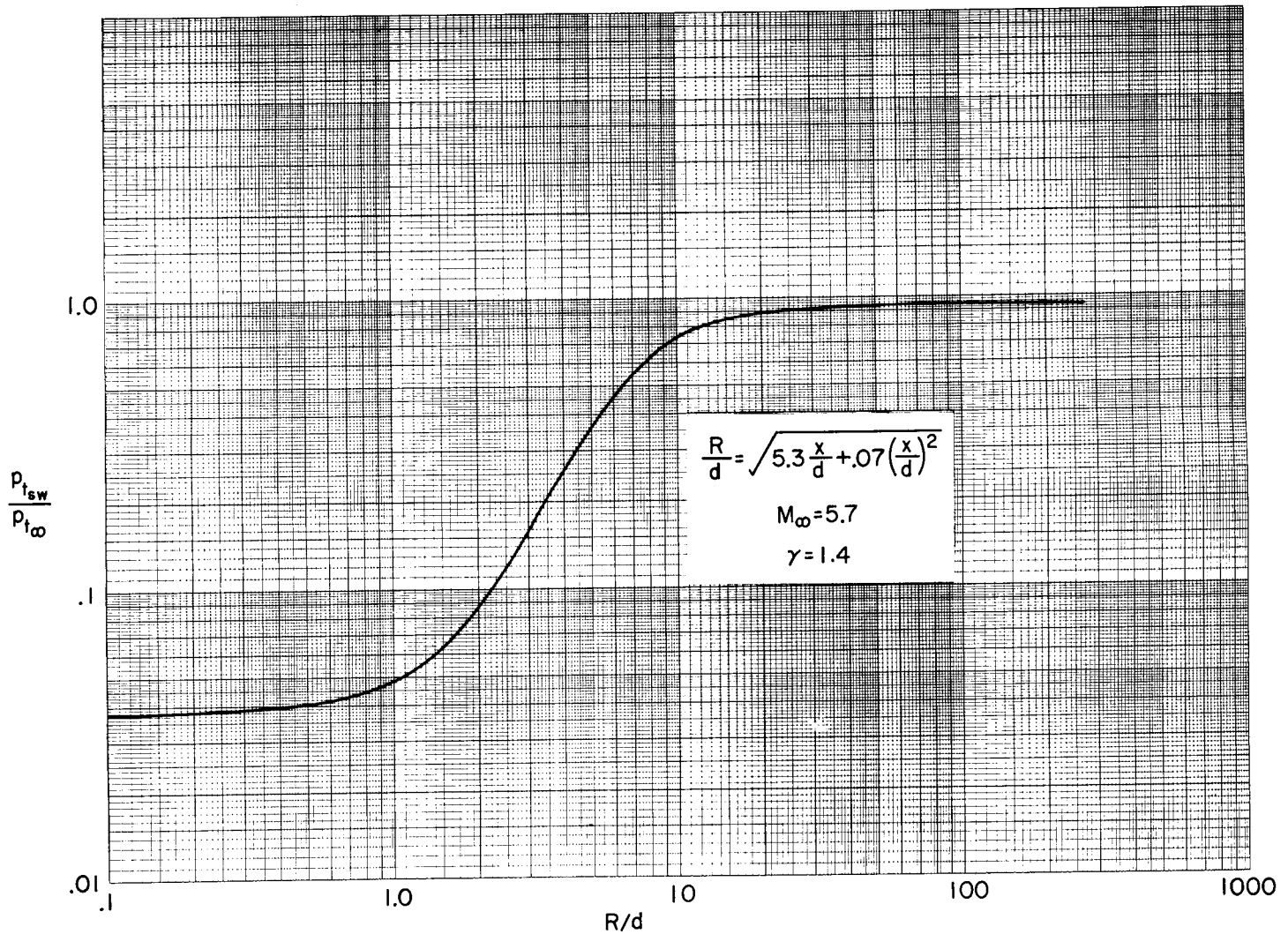

Figure 9.- Calculated variation of total-pressure ratio across the measured shock wave with ratio of shock-wave height (above plate center line) to leading-edge thickness.

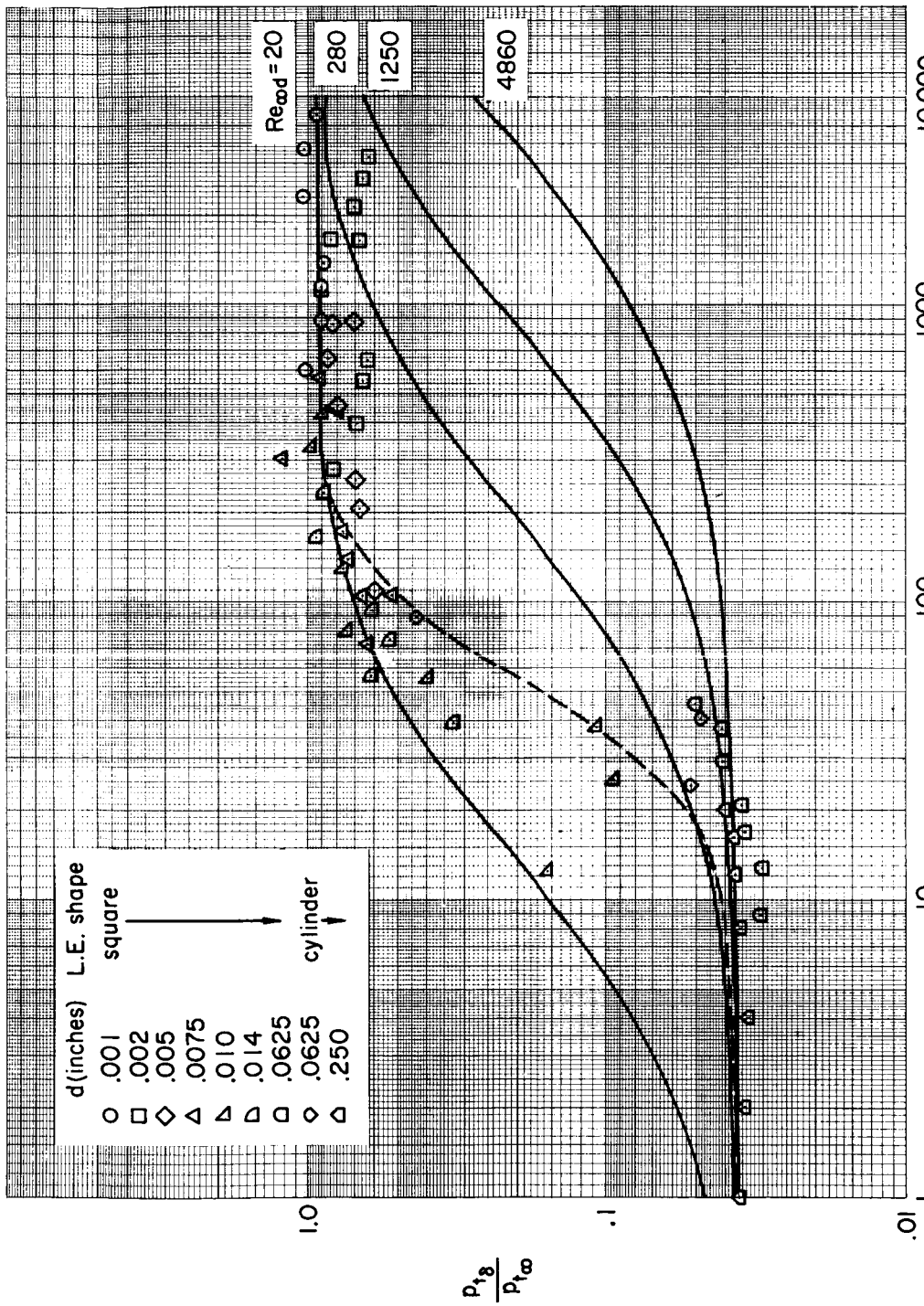

Figure 10.- Variation of boundary-layer-edge total pressure with distance from leading edge; $M_\infty = 5.7$, $Re_\infty = 20{,}000$ per inch.